Ocean Sci. Discuss., 8, 2271–2311, 2011
www.ocean-sci-discuss.net/8/2271/2011/
doi:10.5194/osd-8-2271-2011

Ocean Science Discussions

Improvements to the PhytoDOAS method for identification of major phytoplankton groups using hyper-spectral satellite data

A. Sadeghi[1], T. Dinter[1,2], M. Vountas[1], B. Taylor[2], I. Peeken[2,3], and A. Bracher[1,2]

[1]Institute of Environmental Physics, University of Bremen, Bremen, Germany
[2]Alfred-Wegener-Institute for Polar and Marine Research, Bremerhaven, Germany
[3]MARUM (Center for Marine Environmental Sciences), Bremen, Germany

Received: 19 October 2011 – Accepted: 6 November 2011 – Published: 23 November 2011

Correspondence to: A. Sadeghi (sadeghi@iup.physik.uni-bremen.de)

Published by Copernicus Publications on behalf of the European Geosciences Union.

Abstract

The goal of this study was to improve PhytoDOAS, which is a new retrieval method for quantitative identification of major Phytoplankton Functional Types (PFTs) using hyper-spectral satellite data. PhytoDOAS is an extension of the Differential Optical Absorption Spectroscopy (DOAS, a method for detection of atmospheric trace gases), developed for remote identification of oceanic phytoplankton groups. Thus far, PhytoDOAS has been successfully exploited to identify cyanobacteria and diatoms over the global ocean from SCIAMACHY (SCanning Imaging Absorption spectroMeter for Atmospheric CartograpHY) hyper-spectral data. The main challenge for retrieving more PFTs by PhytoDOAS is to overcome the correlation effects between different PFTs' absorption spectra. Different PFTs are composed of different types and amounts of pigments, but also have pigments in common, e.g., chl-*a*, causing correlation effects in the usual performance of the PhytoDOAS retrieval. Two ideas have been implemented to improve PhytoDOAS for the PFT retrieval of more phytoplankton groups. Firstly, using the fourth-derivative spectroscopy, the peak positions of the main pigment components in each absorption spectrum have been derived. After comparing the corresponding results of major PFTs, the optimized fit-window for the PhytoDOAS retrieval of each PFT was determined. Secondly, based on the results from derivative spectroscopy, simultaneous fit of PhytoDOAS has been proposed and tested for a selected set of PFTs (coccolithophores, diatoms and dinoflagllates) within an optimized fit-window. The method was then applied to the processing of SCIAMACHY data over the year 2005. Comparisons of the PhytoDOAS PFT retrievals in 2005 with the modeled PFT data from the NASA Ocean Biochemical Model (NOBM) showed similar patterns in their seasonal distributions for diatoms and coccolithophores, especially in the northern parts of the global ocean. The seasonal patterns of the PhytoDOAS coccolithophores indicated very good agreement with the global distributions of Particulate Inorganic Carbon (PIC) provided by MODIS (MODerate resolution Imaging Spectroradiometer)-Aqua level-3 products. Since PIC is known as a proxy for the

abundance of coccolithophores (in open ocean), the latter agreement indicates the basic functionality of the method in retrieving coccolithophores. Moreover, as a case study, the simultaneous mode of PhytoDOAS has been applied to SCIAMACHY data for detecting a coccolithophore bloom around New Zealand (reported by NASA from MODIS imagery in December 2009); the result was quite consistent with the MODIS RGB image and the MODIS PIC map of the bloom, indicating the functionality of the method in short-term retrievals.

1 Introduction

Marine phytoplankton play an important role in the marine ecosystems as the basis of the ocean food chain. Phytoplankton are the main oceanic primary producers and have major contribution to the global carbon cycle by acting as a biological pump for carbon in the ocean (Raven and Falkowski, 1999). Via photosynthesis dissolved carbon dioxide is taken up and released as organic carbon to ocean environment, where it can sink down directly or indirectly through other trophic levels to the ocean floor, or just be recycled in the upper ocean. The most suitable approach to monitor the global distribution of marine phytoplankton and to estimate their total biomass is the use of satellite data (e.g., Platt and Sathyendranath, 1988), which corresponds to the field of ocean-color remote sensing. Using ocean-color sensors, long-term records of aquatic parameters are provided remotely on a global scale, which have different applications (McClain, 2009), e.g., to improve the understanding of ocean biogeochemistry and marine ecosystem dynamics; to assess fisheries productivity and the distribution of harmful algal blooms; and to be used as input data for ocean modeling. In retrieving phytoplankton biomass, most bio-optical ocean-color algorithms (e.g., O'Reilly et al., 1998), derive the concentration of chlorophyll-*a*, (chl-*a*). The reason is that chl-*a* is a common photosynthetic pigment among all phytoplankton species (Kirk, 1994), and therefore is generally used as the measure of phytoplankton biomass (Falkowski et al., 1998). However, aside from chl-*a*, remote identification of phytoplankton functional

types, PFTs, has also been of interest through several distinct attempts, because of the specific biogeochemical impact of different phytoplankton groups (see summary by Nair et al., 2008). These attempts have been done for several purposes, from space-borne detection of harmful algal blooms (Millie et al., 1997) and global-scale mapping of dominant phytoplankton groups (Alvain et al., 2005) to the improvement of the accuracy of satellite-derived chl-*a* in waters with multiple dominating phytoplankton populations (Morel, 1997; Sathyendranath et al., 2004; Aiken et al., 2008). As major ocean color methods rely completely or partly on empirical approaches (e.g., the global method of OC4V4 by O'Reilly et al., 2000 or regionally improved methods such as Arrigo et al., 1998), most studies to derive PFTs from space are also connected to these algorithm principles, which relate satellite remote-sensing reflectance (R_{rs}) to in-situ geophysical parameters. Using additional sets of in-situ data, including regional distributions of PFTs and optical parameters, these studies connect the changes observed in optical parameters to the variations measured in pigment compositions, cell size and phytoplankton populations (Alvain et al., 2005, 2008; Aiken et al., 2007). Some studies have suggested the application of a regionally parameterized algorithm instead of the universal retrieval algorithm (Sathyendranath et al., 2004).

Nevertheless, the fact that all these attempts are more or less dependent on large sets of a-priori in-situ measurements has motivated the development of an alternative method in this field, called PhytoDOAS (Bracher et al., 2009), which is essentially different from the well-known ocean-color algorithms and uses the whole spectral information on a large wavelength range, instead of using just a few wavelength bands reflectance data. Using this method, global distribution of two major PFTs, diatoms and cyanobacteria, have been quantitatively derived by Bracher et al. (2009) from the data provided by SCIAMACHY, a hyper-spectral satellite sensor on-board ENVISAT. The study presented here is dedicated to improving the PhytoDOAS method in order to discriminate more PFTs from SCIAMACHY data. PhytoDOAS as an extension of Differential Optical Absorption Spectroscopy, DOAS (Perner and Platt, 1979), to the aquatic medium, is based on using differences in spectral features of absorption spectra of

major PFTs in order to discriminate between them. Distinguishing fine spectral differences in absorption effects of different PFTs over a wide wavelength range requires to utilize a hyper-spectral sensor. However, contrary to the distinctive spectral behaviors in absorption spectra of atmospheric trace gases – which make them fairly straightforward targets to be discriminated by DOAS –, absorption spectra of phytoplankton species contain strong spectral correlation in any operating wavelength window. This fact is a challenge in the retrieval of phytoplankton functional types by this method. Therefore, in this study solutions to this challenge are discussed. The resulting maps corresponding to these approaches, showing the global distribution and seasonal variation of two other PFTs, i.e., *Emiliania huxleyi* (*E. huxleyi*) and dinoflagellates, are presented.

2 Material and methods

2.1 From DOAS to PhytoDOAS

PhytoDOAS, the retrieval method to derive the quantitative distribution of various phytoplankton groups, is an extension of DOAS (Perner and Platt, 1979) from the atmospheric domain into the aquatic media. DOAS expands the *Beer-Lambert* law to all possible interactions between light and all atmospheric optical components. Therefore, it contains all extinction impacts of the atmosphere, including the absorption and scattering by trace gases (scattering is negligible) and scattering of the air molecules, as Rayleigh and Mie scattering. The extension of the original form of *Beer-Lambert* law, Eq. (1), to its applicable form in the atmosphere, is outlined as follows:

$$I(\lambda) = I_0(\lambda) \cdot \exp\left\{ -L \sum_{i=1}^{N} (a_i(\lambda) + s_i(\lambda)) n_i \right\} \quad (1)$$

with $I(\lambda)$ and $I_0(\lambda)$ being the measured intensities for the incident and the transmitted radiations, respectively; $a_i(\lambda)$ and $s_i(\lambda)$ being the absorption and the scattering

cross-sections [$\mathrm{cm}^2\,\mathrm{mol}^{-1}$] of the ith species, accounting together for the *extinction cross-section*; n_i as the number density of the ith species [$\mathrm{mol\,m}^{-3}$]; L as the length total light-path and λ as the wavelength. Here the positive dimensionless argument of the exponential function, $L \sum_{i=0}^{N} (a_i(\lambda) + s_i(\lambda)) n_i$, is called the *optical depth* (or the *optical thickness*) of the medium, mostly denoted by τ. Now, to modify this equation for the atmospheric applications, Rayleigh and Mie scattering of the air molecules have to be taken into account. By implementing the above points into Eq. (1) and integrating over the whole atmospheric light-path, the following equation is obtained:

$$\begin{aligned} \tau(\lambda) &= \ln \frac{I_0(\lambda)}{I(\lambda)} \\ &= \int \left[\sum_{i=1}^{N} \sigma_i(\lambda) \rho_i(s) + \sigma^{\mathrm{R}}(\lambda) \rho^{\mathrm{R}}(s) + \sigma^{\mathrm{M}}(\lambda) \rho^{\mathrm{M}}(s) \right] ds \end{aligned} \quad (2)$$

where ds is the light-path differential element; $\sigma^{\mathrm{R}}(\lambda)$ and $\sigma^{\mathrm{M}}(\lambda)$ are the scattering cross-sections assigned to Rayleigh and Mie scattering, respectively; $\rho^{\mathrm{R}}(s)$ and $\rho^{\mathrm{M}}(s)$ are the number densities associated with Rayleigh and Mie scattering in the atmosphere. Thus the last two terms in Eq. (2) correspond to the Rayleigh and Mie *extinction coefficients*. As another modification, the absorption contributions of different trace gases have been added into Eq. (1) via a summation term, $\sum_{i=0}^{N} \sigma_i(\lambda) \rho_i(s)$, which is a valid treatment as long as the atmosphere is *optically thin*, i.e., $\tau \ll 1$. Each trace gas in Eq. (2) has an absorption cross-section of $\sigma_i(\lambda)$ and a number-density of $\rho_i(s)$.

If the absorption cross-sections do not vary along the light-path, the total amount of the absorber per unit area integrated along the light-path through the atmosphere can be defined as the *slant column density*, SC_i, which has the unit of [$\mathrm{mol\,cm}^{-2}$]:

$$\mathrm{SC}_i = \int \rho_i(s) ds \quad (3)$$

Now, incorporating the *slant column density*, Eq. (2) is modified as follows:

$$\tau(\lambda) = \ln\frac{I_0(\lambda)}{I(\lambda)} = \{\sum_{i=1}^{N}\sigma_i(\lambda)\mathrm{SC}_i + \sigma^{\mathrm{R}}(\lambda)\mathrm{SC}^{\mathrm{R}} + \sigma^{\mathrm{M}}(\lambda)\mathrm{SC}^{\mathrm{M}}\} \quad (4)$$

with SC_i being the *slant column density* of the ith trace gas; and SC^{R} and SC^{M} being the slant column densities of Rayleigh and Mie scattering, respectively. The absorption cross-section for any specific species can be split into two components, one slowly-varying with wavelength, $\sigma_i^s(\lambda)$, and the other rapidly-varying, $\sigma_i'(\lambda)$, called *differential cross-section*:

$$\sigma_i(\lambda) = \sigma_i'(\lambda) + \sigma_i^s(\lambda) \quad (5)$$

These two spectral components can be calculated through several separation techniques, e.g., subtraction of a fitted polynomial, which is equivalent to the high-pass filtering. As shown in Fig. 1, by subtracting a low-order polynomial, the slowly-varying spectral component can be removed, resulting in the differential cross-section. The separation of cross-sections, is implemented in Eq. (4), to split the right-hand side of the equation into rapidly-varying and slowly-varying parts. Meanwhile, the fact that the scattering efficiencies of Rayleigh and Mie scattering exhibit slow-varying dependence with wavelength (as follows):

$$\sigma^{\mathrm{R}}(\lambda) \propto \lambda^{-4} \quad (6)$$

$$\sigma^{\mathrm{M}}(\lambda) \propto \lambda^{-\kappa};\ \kappa = 0\ldots2 \quad (7)$$

implies that the last two terms in Eq. (4), corresponding Rayleigh and Mie scattering, must be inserted in the slowly-varying part. Accordingly, Eq. (4) can be rewritten as:

$$\tau(\lambda) = \ln\frac{I_0(\lambda)}{I(\lambda)} = \underbrace{\{\sum_{i=1}^{N}\sigma_i'(\lambda)\mathrm{SC}_i\}}_{\text{rapidly varying}} + \underbrace{\{\sum_{i=1}^{N}\sigma_i^s(\lambda)\mathrm{SC}_i + \sigma^{\mathrm{R}}(\lambda)\mathrm{SC}^{\mathrm{R}} + \sigma^{\mathrm{M}}(\lambda)\mathrm{SC}^{\mathrm{M}}\}}_{\text{slowly varying}} \quad (8)$$

Now, assuming that there is a low-order polynomial, denoted by $\sum b_{\mathrm{p}}\lambda^{\mathrm{p}}$, covering the slowly-varying part of Eq. (8), this equation can be modified again in the following manner:

$$\tau(\lambda) = \ln\frac{I_o(\lambda)}{I(\lambda)} = \sum_{i=1}^{N}\sigma_i'(\lambda)\mathrm{SC}_i + \sum_{\mathrm{p}=0}^{M} b_{\mathrm{p}}\lambda^{\mathrm{p}} \quad (9)$$

This is the basic equation to establish the DOAS retrieval method. The radiation spectra, I_0 and I, are measured by the satellite sensor (or ground-based instruments) and the absorption cross-sections of trace gases, $\sigma_i(\lambda)$, are measured in the laboratory and then their differential parts are extracted. The *least square* optimization method is used to fit the parameters assigned to the slant column densities, SC_i and the polynomial coefficients, b_{p}. The main underlying idea in this optimization approach is to fit the parameters SC_i and b_{p}, in accordance with the demand of minimizing the residuals. Therefore, the DOAS retrieval method can be introduced by this expression:

$$\left\| \tau(\lambda) - \sum_{i=1}^{N}\sigma_i'(\lambda)\mathrm{SC}_i - \rho'(\lambda)S_{\mathrm{r}} - \sum_{\mathrm{p}=0}^{M} b_{\mathrm{p}}\lambda^{\mathrm{p}} \right\|^2 \rightarrow \min \quad (10)$$

Here, to incorporate the main atmospheric constituents, a new term, $S_r\rho'(\lambda)$, has been added into the equation, accounting for the spectral impact of the Ring effect. The Ring effect is the inelastic scattering of air molecules associated with the rotational Raman scattering. As the rotational Raman scattering has a *filling-in* impact on the Fraunhofer lines in the UV-visible range (Bussemer, 1993; Burrows et al., 1995), it must be accounted for in the DOAS equation to compensate its weakening impact onto the measured absorption lines (Vountas et al., 1998, 2007; Wagner et al., 2001) and correcting the absorption lines of trace gases within the overlapping bands with the Ring spectral domain. Therefore, within the DOAS equation (Eq. 10), the impact of the Ring effect is referred to as a *pseudo-absorber*. To incorporate the Ring effect into the DOAS retrieval, a unitless spectral reference of the Ring, $\rho(\lambda)$, has been computed from a method developed by Vountas et al. (1998), based on modeling of radiative transfer. In the above equation, $\rho'(\lambda)$ corresponds to the differential part of the Ring spectrum. The associated coefficient within the term of the Ring effect, i.e., S_r, is called the Ring *fit-factor*, which is unitless like the spectral signature of the Ring effect.

PhytoDOAS was born, when the DOAS method was applied for retrieving oceanic phytoplankton, as the living light-absorber particles of the water medium. The underlying idea is that the backscattered light from the ocean into the atmosphere (and hence, to the satellite sensor), carries some information from water and its optical constituents. The method was established by Vountas et al. (2007) for remote identification of total phytoplankton chl-*a* and then improved by Bracher et al. (2009) to identify diatoms and cyanobacteria in *case-I* waters using hyper-spectral satellite data. Such an extension demands the incorporation of all optical components of the sea water into the DOAS equation, based on a prior knowledge of the optical behavior of the main constituents. In addition to phytoplankton, the main optical components of case-I waters, the target area of the method, are CDOM (colored dissolved organic matter), non-algal particulates, absorption of water molecules (Gordon et al., 1975; Kirk, 1994) and Vibrational Raman Scattering (VRS) of liquid water, which is an inelastic scattering effect of water molecules (Vasilkov et al., 2002b; Vountas et al., 2003).

Both absorption and scattering of CDOM have a spectrally smooth behavior (Bricaud et al., 1981; Carder et al., 1989), which leads them to be covered in the DOAS equation by the fitted polynomial. The same condition governs the absorption and scattering of the non-algal particulates (Allali et al., 1995; Mitchell et al., 2003). The absorption effect of water molecules can be regarded as a fixed spectral background, which can be removed from the main DOAS fit by an initial run of the method over a phytoplankton-depleted oceanic region, so-called *hyper-oligotrophic water*; this initial run will remove some instrumental artifacts as well. According to Vountas et al. (2003, 2007) backscatter radiation detected by SCIAMACHY sensor carries the spectral footprint of inelastic scattering, VRS, of water molecules. The spectral impact was quantitatively shown using the DOAS method, by embedding the spectral signature of VRS, $v(\lambda)$ as a pseudo-absorber, into the DOAS equation (Eq. 10). It was shown in Vountas et al. (2007) that there is a strong relation between VRS and *light-penetration depth*, suggesting the former to be used as a proxy for quantitative estimation of the latter. Therefore, to extend the DOAS for retrieving chl-*a* concentration of a PFT, the VRS reference spectrum must be in parallel fitted (as a pseudo-absorber) in the UV range, which is used later for computing the *light-penetration depth* for each satellite ground pixel. Finally, to extend the DOAS equation into the aquatic medium, the absorption spectrum of target PFT has to be considered. Now, embedding the two new terms representing the PFT absorption spectrum and the VRS reference spectrum, the relevant equation for PhytoDOAS is achieved as follows:

$$\left\| \tau(\lambda) - \sum_{i=1}^{N} \sigma_i'(\lambda)\mathrm{SC}_i - \rho'(\lambda)S_r - a'(\lambda)S_a - v'(\lambda)S_v - \sum_{p=0}^{M} b_p\lambda^p \right\|^2 \rightarrow \min \quad (11)$$

with $a'(\lambda)$ being the differential part of *specific absorption spectrum* of target PFT (absorption spectrum of the PFT sample normalized by its measured chl-*a* concentration)

in [m^2 (mg chl-a)$^{-1}$]; S_a being the *fit-factor* of the PFT absorption spectrum in [mg chl-a m^{-2}]; $v'(\lambda)$ being the differential part of the VRS spectrum, which was obtained from a reflectance model developed by Vountas et al. (2003), originally proposed by Sathyendranath and Platt (1998); and S_v being the *fit-factor* assigned to the VRS spectrum. It must be noted that since $a'(\lambda)$ is not an absorption cross-section, the absorption fit-factor, S_a, has a different interpretation than in slant-column density. The PFT absorption fit-factor implies the mass per unit area of chl-*a* pigment assigned to the target PFT along the light-path. However, as the spectral signature of VRS is unitless (Vountas et al., 2007), the VRS fit-factor, S_v, is unitless as well, similar to the fit-factor of the other *pseudo-absorber*, i.e., of the Ring spectrum.

The main outputs of PhytoDOAS are S_a and S_v, which are retrieved independently through two separate fit processes. Since VRS spectral features are weak in the visible, whereas the absorption features of PFTs are fitted in visible, the second fit is done for evaluating the VRS fit-factor in UV range, which is then extrapolated to the visible (Bartlett et al., 1998; Vountas et al., 2003, 2007).

Regarding the PhytoDOAS equation (Eq. 11), three sets of input data are needed to perform this method, being as follows: (1) satellite measurements, i.e., extraterrestrial solar irradiace, $I_0(\lambda)$, and Earth's backscattered radiation, $I(\lambda)$, both measured by the satellite sensor at the top of the atmosphere, to be embedded into the optical depth, through $\tau(\lambda) = \ln\frac{I_0(\lambda)}{I(\lambda)}$; (2) atmospheric spectra, i.e., absorption cross-sections of water vapor, trace gases and spectral signature of the Ring effect; and (3) aquatic spectra, i.e., specific absorption spectrum of the PFT and the spectral signature of VRS. As a recent improvement to PhytoDOAS, presented in this study, instead of just a single PFT target, three selected PFT targets are fitted simultaneously. This new approach is referred to as *multi-target fit* in this study (see Sect. 2.4). Accordingly, to incorporate the *multi-target fit* in PhytoDOAS, the term of PFT absorption in Eq. (11), i.e., $a'(\lambda)S_a$, must be replaced by a multiple term containing the absorption spectra of the selected PFTs; within this multiple absorption term, $\sum_{j=1}^{3} a'_j(\lambda)S_{aj}$, a certain absorption fit-factor is assigned to each PFT target. Therefore, the improved PhytoDOAS can be introduced

by this expression:

$$\left\| \tau(\lambda) - \sum_{i=1}^{N} \sigma'_i(\lambda)\mathrm{SC}_i - \rho'(\lambda)S_r - \sum_{j=1}^{3} a'_j(\lambda)S_{aj} - v'(\lambda)S_v - \sum_{p=0}^{M} b_p\lambda^p \right\|^2 \rightarrow \min \quad (12)$$

Vountas et al. (2007) showed that the light-penetration depth, δ, can be determined using the VRS fit-factor. For water molecules, a single event of elastic scattering is always accompanied by an inelastic scattering of VRS. Therefore, the VRS fit-factor, S_v, is directly related to the same quantity of elastic scattering of water molecules, which is described by the *backscattering coefficient*, b_b. The quantitative dependence was previously extracted in Vountas et al. (2003) using a bio-optical model from Morel (1988), stating that the backscattering coefficient scaled by VRS fit-factor, S_v, can be regarded as the true value of b_b in the observed situation. Therefore, as b_b^{-1} is the modeled *light-penetration depth*, $S_v \cdot b_b^{-1}$ will be the equivalent observed quantity. Here, the *light-penetration depth*, denoted by δ, refers to the depth of the remotely observed water column, up to which the signal can be received by satellite sensor. However, since δ is wavelength-dependent, an average value of it over the used wavelength band is computed for each ground pixel.

As explained in Vountas et al. (2007) and Bracher et al. (2009), the chl-*a* concentration of the target PFT can be estimated from the PFT absorption fit-factor, S_a, determined via PhytoDOAS. This is done for all ground pixels through dividing S_a by the *light-penetration depth* and can be written as follows:

$$C = \frac{S_a}{\delta} \quad (13)$$

Where C is the chl-*a* concentration of the target PFT, [mg m^{-3}].

In PhytoDOAS (as in DOAS), the overall *Chi-square* value, χ^2, is used as a scalar indicator of the total fit-quality. Furthermore, the fit spectrum of the retrieval target is compared with its original spectrum for each oceanic pixel to check the fit-quality. However, as in any other retrieval method, the most reliable approach to investigate the quality of PhytoDOAS retrieval is the validation with high quality in-situ PFT data.

2.2 Satellite data

As mentioned before, due to spectral correlation of phytoplankton absorption features, satellite data used in PhytoDOAS must be highly spectrally resolved. To meet this requirement, data measured by the satellite sensor SCIAMACHY (SCanning Imaging Absorption spectroMeter for Atmospheric CHartographY), which is on board ENVISAT (ENVIronmental SATellite of European Space Agency, ESA) launched in 2002, are used in this study. SCIAMACHY, originally designed for atmospheric measurements, covers a wide wavelength range (from 240 nm to 2380 nm in eight channels), which makes it an ideal sensor for the detection of aerosols and clouds, as well as being suitable for several retrieval methods of trace gases. Beside the large wavelength range, covering UV/Visible/NIR, this sensor can observe an air volume from three different viewing angles (nadir, limb and sun/moon occultation), leading to precise atmospheric data on vertical column densities and profile information. Furthermore, the instrument benefits from a relatively high spectral resolution, ranging from 0.2 nm to 1.5 nm for its scanning channels over the range 240 nm to 1700 nm, and also selected regions between 2000 nm and 2400 nm (Bovensmann et al., 1999). In this study, the SCIAMACHY data in UV and visible regions, from nadir-viewing geometry with a spectral resolution of 0.24 nm to 0.48 nm, have been used. These data correspond to backscatter solar radiation from the Earth's surface, with the spatial resolution of about 30 km × 60 km, which defines the pixel-size in this wavelength region. Each ground pixel data is associated with a direct measurement of solar radiation at the top of the atmosphere in the same wavelength region, to be used later in the retrieval as the unattenuated radiation,

I_0 (see Eq. 9). Within PhytoDOAS, SCIAMACHY data are used in the two following steps: first, SCIAMACHY visible data are used to fit the absorption spectrum of target PFT within the wavelength range of 429 nm to 495 nm in the study by Bracher et al. (2009) and extended up to 521 nm in this study, leading to PFT absorption fit-factors; secondly, SCIAMACHY data from 340 to 385 nm are exploited to fit the VRS spectral signature of water molecules, leading to the VRS fit-factors, which are necessary for the calculation of the light-penetration depth for each oceanic pixel (see previous section).

Moreover, MODerate resolution Imaging Spectroradiometer (MODIS)-Aqua level-3 products were used to obtain the seasonal composites of Particulate Inorganic Carbon (PIC) in a 9 km grid during spring and summer 2005 (The MODIS algorithm for PIC has been described in Balch et al., 2005). Since coccolithophores are the main planktonic producer of calcium carbonate, suspended PIC in open ocean is an indicator of coccolithophores (Balch et al., 2005), the PhytoDOAS retrievals of coccolithophores was compared to the global distribution of PIC. For the same reason, in detection of a certain coccolithophore bloom as a case study, a weekly composite of MODIS-Aqua PIC (in December 2009) has been used to test the respecting result of PhytoDOAS.

2.3 Spectral data

In addition to hyper-spectral satellite radiation measurements, the PhytoDOAS retrieval requires reference spectra of atmospheric and oceanic species. For atmospheric spectra, absorption cross-sections of ozone, NO_2, glyoxal or OCHCHO, iodine oxide, O_4, water vapor and the Ring effect (as a *pseudo-absorber* spectrum) are fitted, using the same spectra as were taken in Bracher et al. (2009).

The second set of input parameters includes the spectral signature of VRS, obtained through a modeling approach (Vountas et al., 2003, 2007) and the absorption spectra of PFTs. It must be mentioned that as *E. huxleyi* is the dominant species of the coccolithophores, it has been used in this study as the spectral indicator of this PFT target. The phytoplankton absorption spectra used in this study were acquired from

an *E. huxleyi* culture and a natural sample, where the group of dinoflagellates dominated. Both samples were measured with a point-source integrating-cavity absorption meter, so-called PSICAM (Roettgers et al., 2007). Total chl-*a* concentrations of the *E. huxleyi* culture and of all pigments for the natural dinoflagellate sample were obtained from high-performance liquid chromatography (HPLC) following the method described by Hoffmann et al. (2006). The dinoflagellate dominated sample was taken during the OOMPH field experiment (Organics over the Ocean Modifying Particles in both Hemispheres) with RV Marion Dufresne on 2 February 2007, at 59.88° W and 46.01° S, within a dinoflagellate bloom. Performing the CHEMTAX analysis (Mackey et al., 1996) on the HPLC data of the natural sample, the chl-*a* concentrations of all containing phytoplankton groups were calculated, which indicated a contribution over 92 % for the dinoflagellates. The rest of the sample consisted of 5 % pelagophyceae and less than 3 % of prasinophyceae (further details in Yassaa et al., 2008). To derive the specific absorption spectra of each phytoplankton group, each absorption spectrum was divided by the corresponding chl-*a* concentration (normalization). Additionally, as the third phytoplankton reference spectrum, the absorption spectrum of diatoms was acquired from the in-situ measurements conducted during a cross-Atlantic research cruise. The process to reach the specific absorption spectrum of diatoms was the same as the one explained for dinoflagellates (for details see Bracher et al., 2009).

Figure 2 (left panel) shows the specific absorption spectra of the three PFTs used as the retrieval targets in this study, i.e., for *E. huxleyi*, dinoflagellates and diatoms. From these measured spectra, the corresponding differential absorption spectra have been derived, based on the separation approach described in the method section (see Sect. 2.1). The differential absorption spectra for the selected phytoplankton targets are depicted in the right panel.

2.4 Improvements to PhytoDOAS: challenges and approaches

Following the method by Bracher et al. (2009), besides cyanobacteria and diatoms, more major PFTs (or dominant species of a PFT) are expected to be retrieved.

Nevertheless, there are some challenges to be overcome in order to improve PhytoDOAS to be a reliable retrieval tool for other PFTs (or dominant species). The main challenge is the spectral correlation between absorption spectra of different phytoplankton targets, which arises from their common photosynthetic pigments and causes in turn difficulties to distinguish different groups remotely. In this study, several approaches have been applied to overcome the correlation found among typical PFTs' absorption spectra. Firstly, investigations proved that fitting several PFTs' spectral targets simultaneously, within an appropriate fit-window, leads to higher fit-quality as compared to fit only one PFT spectrum at the time. This approach, called as *multi-target fit*, results in significantly lower values for the absorption fit-factors of each target, compared to the usual approach of single-target fit. This is of importance, because high fit-factors in PhytoDOAS lead to an overestimation of the PFT concentration. This can be explained by the fact that when three (or more) PFT targets are ïtted simultaneously, the phytoplankton spectral input of the PhytoDOAS equation becomes bio-optically more realistic; i.e., in this case PhytoDOAS accounts for more optical components of the ocean water, which usually contains simultaneously several types of phytoplankton species. Comparably, when we omit some trace gases from our DOAS retrieval, the retrieval results of the others are affected. Figure 3 shows different fit-factor results obtained for *E. huxleyi* by following single-target fit and triple-target fit modes of PhytoDOAS (the triple-target fit includes *E. huxleyi* together with diatoms and dinoflagellates). The triple-target fit results (Fig. 3 lower panel) are characterized by lower values of fit-factors, almost over the whole global ocean, as compared to the single-target fit results (Fig. 3 upper panel). This is in a better agreement with the coccolithophore chl-*a* data achieved by the NASA Ocean Biochemical Model, NOBM (Gregg et al., 2003; Gregg and Casey, 2007). Moreover, the results are also verified by looking at the fit residuals, as a measure of the fit-quality, represented by the average value of *Chi-square* (χ^2) for all accounting pixels. Since the lower residual corresponds to the more reliable fit, the lower average of χ^2 values in the triple-target fits, compared to the single-target fits, implies the privilege of the triple-target fits. In the sample fit-factor

maps shown in Fig. 3, the average χ^2 values for the triple-target and single-target fits are 0.00039 and 0.00052, respectively (see also the comparison of overall residuals in Fig. 5).

However, due to the limitations imposed by the spectral correlation, it is necessary to determine and optimize some factors when running a multi-target fit, in order to receive an acceptable fit-quality: the retrieval should be optimized by identifying how many PFT targets, in which combination and within which wavelength window are fitted simultaneously. Various methods have been used to investigate the fit-quality in each tested option as follows:

1. Comparison of the overall averaged *Chi-square* values of the different fit results.
2. Comparison of the fit absorption spectra with the input spectra for selective pixels.
3. Comparison with the available high quality in-situ measurements.

The last option is the most reliable criterion to check the results' fit-quality, but it could not always be followed. Reasons for that are the too limited availability of in-situ data with a global distribution of major PFTs and also the difficulties associated with the co-location (matching) of satellite ground pixels to the existing in-situ data due to the large pixel size. As an initial step to validate our PFT retrieval results, we compare our PFTs' retrieval results to the NOBM modeled data of PFTs' global distribution (see Sect. 3.2).

As a complementary approach, the spectral behavior of PFTs' absorption spectra have been investigated in more detail, using *fourth-derivative spectroscopy* (according to Aguirre-Gomez et al., 2001), which is a well-known method in spectral studies of phytoplankton species. The core concept here is as follows: in the forth-derivative curve of a given absorption spectrum, each peak corresponds to the maximum absorption for a specific pigment at the same wavelength position. Therefore, the distribution of peak positions in a forth-derivative curve is an indicator of pigment composition for that PFT. Figure 4 shows the fourth derivative curves for the absorption spectra of three phytoplankton targets, which have been fitted simultaneously via PhytoDOAS.

The fourth-derivative method can be used to identify tiny differences in PFTs' spectral behavior. This is helpful to avoid spectral correlations between different phytoplankton targets and to find the appropriate wavelength window to fit them simultaneously. As shown in Fig. 4, there is a spectral difference between target spectra in the interval from 495 nm to 521 nm, especially between diatoms and *E. huxleyi*, for which the spectral behavior are more alike in the wavelengths below 495 nm. Practically, in the simultaneous PhytoDOAS fit, the spectral differences seen in the fourth derivative curves have been used (as one criterion) to select the set of PFT targets, i. e., the proper combination of PFTs, and also to specify the wavelength range of the actual fit-window. This explains why in this study a wider fit-window (429 nm to 521 nm) has been used than in Bracher et al. (2009), which was from 429 nm to 495 nm.

All together, it was determined so far that among all tested options of PhytoDOAS multi-target fit (which was previously shown to have better result than single-target fit), following configuration leads to the best fit-quality: the PhytoDOAS triple-target fit containing absorption spectra of diatoms, dinoflagellates and *E. huxleyi* over the wavelength window of 429 nm to 521 nm.

Figure 5 compares the fit-quality of PhytoDOAS retrieval when being performed in single-target fit mode and in multi-target mode, using the overall fit residuals. It can be seen that the overall residual for the single-target fit (diatoms; in red), almost over the whole fit-window, is higher than for the triple-target fit (diatoms, dinoflagellates and *E. huxleyi*; in green). Furthermore, regarding the DOAS method, this figure also shows that when spectral contribution of phytoplankton absorption is taken into account by DOAS retrieval (over the ocean), the fit-quality will be clearly better; this can be inferred from the obviously higher residual of the retrieval when running without any PFT target (blue curve).

3 Results and discussion

3.1 Monthly averages by multi-target fit

In this section the results of using PhytoDOAS to retrieve *E. huxleyi* and dinoflagellates from SCIAMACHY data 2005 are presented as monthly averages of global chl-*a* distributions. The results were obtained by conducting the triple-target fit mode of PhytoDOAS, with diatoms, *E. huxleyi* and dinoflagellates absorption spectra as the input PFT targets over the wavelength range of 429–521 nm. In this configuration the average value of the overall *Chi-square* was minimal and fit spectra in selected oceanic pixels were in good agreement with the original PFTs' absorption spectra. Figures 6 and 7 show the monthly averaged global distribution of chl-*a* for *E. huxleyi* and dinoflagellates using SCIAMACHY data from March and October 2005.

In each set of these figures, there are clear differences in the distribution of chl-*a* for these two PFT targets. For example, Fig. 6 (March 2005) *E. huxleyi* shows high chl-*a* in the north of the Polar Front and elevated chl-*a* in parts of the tropics and subtropics, while dinoflagellates shows elevated chl-*a* in the North Atlantic and the North Pacific, where *E. huxleyi* chl-*a* is much lower. Furthermore, the temporal variation of patterns for each PFT over the year can be seen by comparing these two sets of chl-*a* maps. For instance, in October, compared to March 2005, averaged chl-*a* of *E. huxleyi* is still high in the north of the Polar Front, while now also the North Atlantic and the North Pacific show high values, which might be explained by the pronounced seasonal cycle of this species in the north. For dinoflagellates in October 2005, chl-*a* is lower in the northern mid and high latitudes as compared to March, whereas it is vice versa for the southern mid and high latitudes. However, it is present in the south in early spring.

3.2 Comparison with modeled data: seasonal averages

In Figs. 8 and 9 the seasonal averages of global distributions of the PhytoDOAS coccolithophores (upper panels) are compared with two available global products

corresponding to coccolithophores: the NOBM modeled data of coccolithophores (middle panels) and the MODIS-Aqua PIC concentration (lower panels). The maps shown in Fig. 8 correspond to the northern spring (April/May/June) and the maps in Fig. 9 correspond to the northern summer (July/August/September) 2005. The PhytoDOAS results, illustrated as chl-*a* conc., have been retrieved via *triple-target fit* from SCIAMACHY data. In the PhytoDOAS fit process *E. huxleyi*, the globally dominant species of coccolithophores, was fitted together with diatoms and dinoflagellates within the fit-window of 429–521 nm. The coccolithophore modeled data, presented as chl-*a* conc., were acquired from the NASA Ocean Biochemical Model (NOBM), which provides time-series of PFT assimilated data. The PIC data were provided by seasonal composites of the MODIS-Aqua level-3 products, presented as conc. of the suspended $CaCO_3$ [mol m^{-3}].

As shown in Figs. 8 and 9, the seasonal distribution patterns of the PhytoDOAS coccolithophores (upper panels) have very good agreement with the PIC distributions (upper panels) in both figures, corresponding to spring 2005 and summer 2005, respectively. The similar patterns for enhanced coccolithophores and PIC not only can be seen on the large scales, e.g., in the North Atlantic, the North Pacific, the belt-like area between the Subtropical Front and the northern parts of Sub-Antarctic Front (in spring 2005), but also are visible on the regional scales, e.g., in the Bering Sea, the Labrador Sea, northern part of the Arabian Sea (in spring 2005), the Arafura Sea (as well as in the Gulf of Carpentaria) and even in the Mediterranean Sea and the Caspian Sea. Nevertheless, the elevated values of the PhytoDOAS coccolithophores in the Mid-Pacific (upper panels in Figs. 8 and 9) can not be seen well in the PIC maps (lower panels), both in spring and summer 2005. Moreover, the elevated values of the PhytoDOAS coccolithophores in the southern parts of the Subtropical Front in summer 2005 (upper panel in Fig. 9) is not as pronounced in the respecting PIC map (lower panel in Fig. 9). Since PIC is known to be a reliable proxy of the abundance of coccolithophores in *case I* waters Balch et al. (2005), the similar patterns mentioned above imply the functionality of the PhytoDOAS improved method in retrieving the coccolithophores. However,

the precise validity test should be done by converting the PIC concentration into the concentration of the living coccolithophore cells, which involves some complexities.

The main complexity is arising from the simultaneous existence of the suspended coccoliths (calcite plates detached from coccolithophores), associated with other factors, e.g., different amounts of $CaCO_3$ existing in each specific type of coccolith plate Balch et al. (2005); different numbers of coccoliths assigned to different species of coccolithophores; etc. Regarding this limitation, other comparisons were conducted using the coccolithophore modeled data provided by NOBM, which are shown in the middle panels of Figs. 8 and 9. Here the distributions of coccolithophores from PhytoDOAS and NOBM indicate similar patterns in the North Atlantic, east of Australia (northern parts of the Tasman Sea), the Mid-Pacific (partly), the tropical regions of the South-Atlantic near South-America (partly), the south-east waters of Africa (more pronounced in spring) and also partly in the western parts of the Mid-Indian Ocean (eastern coast of Africa). Nevertheless, there are also some regions, where the retrieved and model results look totally different. For example, in both sets of figures (spring and summer) the retrieval results suggest high chl-*a* over the North Pacific, while model results show almost nothing in this regions. The same feature can be seen partially in the high latitudes of the Southern Hemisphere and also in the western part of the South America in the Pacific Ocean.

The retrieval results of diatoms via *triple-target fit* have also very similar distributions as compared to the ones, which had been achieved before in Bracher et al. (2009) using the single-target mode of PhytoDOAS within the fit-window of 429–495 nm. The minor differences can be assigned to the widening of the fit-window up to 521 nm and also to the fact that two more PFT spectral targets have been added into the fit. It seems that the increasing effect of the wider fit-window is compensated by the decreasing effect of the simultaneous fit. As an example of the PhytoDOAS retrieval of diatoms in *triple-target* mode, the seasonal average of retrieved diatom chl-*a* is shown in Fig. 10 (upper panel), where it is compared by a diatom chl-*a* map computed by NOBM modeled data over the same period (lower panel in Fig. 10). As shown in this

figure, in most regions (e.g., the North Atlantic, the North Pacific, the South Atlantic and the South Pacific) there is good agreement between the retrieval result and the modeled data, though the comparison is not possible in very high latitudes in the South, where SCHIAMACHY has no coverage.

Regarding the usual uncertainties and roughnesses associated with the current models of PFTs' global distributions, it can not be expected that the PFT modeled data would provide a reliable source for PFT comparisons and validity-tests. However, due to the shortage of PFT in-situ data for a global comparison, and also the possible limitations in collocating the available in-situ data with satellite ground pixels (as in SCIAMACHY, which has a coarse spatial resolution), the modeled data can be used as a preliminary test. In this sense, the agreements shown above between the PhytoDOAS retrieval and the NOBM modeled data is regarded only as an initial approval of the method functionality, demanding more investigation with all available PFT sources. In case of diatoms the PhytoDOAS retrievals had been previously validated by in-situ data in Bracher et al. (2009); and for the retrieved coccolithophores, as discussed before, comparison with the PIC distribution provides an intermediate test, indicating very good agreement in seasonal patterns (Figs. 8 and 9).

3.3 Bloom detection by PhytoDOAS

As mentioned above, since the availability of in-situ data of the PFTs' distributions in global scale is low (or their collocation adaptability is difficult), phytoplankton blooms could provide us the opportunity to test our retrieval method under realistic conditions. However, the available data of these bloom events are mostly qualitative, like satellite RGB images of coccolithophore blooms, making them not being sufficient for a quantitative comparison.

Figure 11 shows an sample case study of detecting a phytoplankton bloom using PhytoDOAS. It corresponds to a coccolithophore bloom over Chatham Rise (South Pacific, east side of New Zealand), reported by NASA on 23 December 2009 (upper panel in Fig. 11). The PhytoDOAS retrieval of this bloom is shown in the middle panel

of Fig. 11. It was obtained from two weeks data of SCIAMACHY (centered at 23 December 2009) via *triple target fit* within the fit-window of 429–521 nm. The retrieval result of the bloom has also been compared to the PIC distribution over that region (lower panel in Fig. 11), which was prepared as a 8-day composite (19–26 December 2009) from MODIS-Aqua level-3 products. As shown in Fig. 11 the bloom is also visible in the PhytoDOAS retrieval as well as in the MODIS-Aqua PIC result. However, the pattern of the bloom in PhytoDOAS is not completely the same as in the MODIS RGB image and the MODIS PIC map. The main reason for this difference is the different time frames operated for detection of this bloom: while the MODIS true-color image is an instantaneous picture, the PhytoDOAS result is a map of averaged chl-*a* retrieved from two weeks data. Only few SCIAMACHY orbits cross this small region at one day, among which a large fraction of attaining pixels are flagged out due to the sensitivity of the retrieval to cloud contamination. The cloud contamination is also the reason for missing a lot of pixels in the eastern parts, where is almost blank in the respecting map. However, the choice of using a two-week time frame for the retrieval has been relying on the fact that a typical coccolithophore bloom lasts a few days, not just one day and therefore, both in the PhytoDOAS map and in the PIC map (with an an eight-day time frame) the bloom is observable pronouncedly. On the other hand by using a wider time-frame, the slight motion and spreading of the bloom over the time (caused by wind, for example) will also affect the retrieval output pattern.

4 Conclusions

PhytoDOAS is a new method to retrieve the biomass of phytoplankton functional types (PFTs) using hyper-spectral satellite data. This method is potentially an alternative to retrieve total phytoplankton biomass from satellite data with higher accuracy by summing up all major PFTs' chl-*a*, accounting for the total chl-*a*. However, to retrieve total phytoplankton biomass, major PFTs distribution should be first determined; hence, this study was aimed to improve PhytoDOAS by retrieving more PFTs (coccolithophores

and dinoflagellates) than the two PFTs identified before by Bracher et al. (2009), i.e., diatoms and cyanobacteria. The main challenge to fulfill the improvement of PhytoDOAS is to overcome the spectral correlation between absorption spectra of target PFTs, which arises from their common pigments. Two approaches have been used in this study to overcome the correlation effects: (1) Fourth-derivative analysis for the recognition of tiny spectral differences between PFTs' spectral, leading to an extended fit-window for retrieving selected PFTs; (2) simultaneous fit of several PFTs in each PhytoDOAS retrieval process, which in practice was applied to three PFTs, including coccolithophores, diatoms and dinoflagellates. Using these approaches, first attempts have been done to obtain global distributions of coccolithophores and dinoflagellates, for which the sample results obtained from SCIAMACHY data in year 2005 were shown as monthly-mean chl-*a* maps. The seasonal averages of coccolithophore chl-*a* retrieved from the improved PhytoDOAS for spring and winter 2005 have been compared with the MODIS-Aqua Particulate Inorganic Carbon (PIC) global distributions and also with the NOBM assimilated product of coccolithophores. The seasonal patterns of the PhytoDOAS coccolithophores showed (almost overall) very good agreement with the PIC distributions, whereas the agreement with modeled data was good only regionally (especially in the northern latitudes). As an example of diatom retrieval by the improved PhytoDOAS, the seasonal average of diatom chl-*a* for summer 2005 was shown, indicating a very good agreement with the respecting result of NOBM modeled data. Unfortunately, no data source for globla distribution of dinoflagellates was found to be used for comparing the PhytoDOAS dinoflagellates with. As a case study, the PhytoDOAS triple-target approach has been applied to detect a coccolithophore bloom reported by NASA in December 2009. Comparisons with NASA RGB image and also with the MODIS-Aqua PIC result over the bloom region confirm strongly the functionality of the PhytoDOAS method in short time-frames, as in detection of coccolithophore blooms.

4.1 Outlook

There are further steps to proceed the improvement of PhytoDOAS as well as to expand its applications, which can be classified as follows: the retrieval quality of PhytoDOAS has to be improved by doing further tests with current PFT targets followed by introducing more PFT reference spectra into the retrieval. The globla disribution of dinoflagellates retrieved by PhytoDOAS must be compared with an appropriate data set of this taxonomic group. The PhytoDOAS method will be applied to the whole available SCIAMACHY data (2002–2010) and will be validated with the collocated HPLC-based in-situ PFT data. Since absorption spectra of PFTs and also of specific species show some spatial variability over the global ocean (Bricaud et al., 1995), one of the main future tasks is to obtain and represent PhytoDOAS retrievals on a regional basis. Doing this task demands applying PhytoDOAS separately on different oceanic biogeochemical provinces (e.g., based on Longhurst, 1998), for each of which the input phytoplankton absorption spectra must be extracted before from the in-situ measurements in that province. Furthermore, a climatology on the PFT distribution can be developed based on the PhytoDOAS SCIAMACHY results. The resulting data set will be useful to various marine biogeochemical and ecosystem studies and models, as well as being a potential basis for a specific phytoplankton absorption climatology based on the global spatially and temporally resolved PFT distribution. This can be applied to improve the common ocean color chl-*a* retrievals. It could also help improve global estimates of biogenic gas emissions resulting from oceanic phytoplankton, e.g., Dimethylsulphide (DMS) production, which is mostly connected to the abundance of coccolithophores (Keller, 1989).

Acknowledgements. We are thankful to ESA, DLR, and the SCIAMACHY Quality Working Group (SQWG) for providing us with SCIAMACHY level-1 data. We thank NASA-GSFC for NOBM modeled data (Giovanni project) and the MODIS RGB picture. Erika Allhusen we thank for her support during in situ data analysis. The authors are grateful to the IPEV/Aerotrace program for logistical support during the Marion Dufresne cruise and also to Rüdiger Röttgers for his valuable comments on phytoplankton ecology and ocean optics. Funding was provided by the HGF Innovative Network Funds (Phytooptics). Funding for TD was supplied via the EU project SHIVA-226224-FP7-ENV-2008-1. This work is a contribution to the "Earth System Science Research School (ESSReS)", an initiative of the Helmholtz Association of German research centers (HGF) at the Alfred Wegener Institute for Polar and Marine Research.

References

Aguirre-Gomez, R., Weeks, A. R., and Boxall, S. R.: The identication of phytoplankton pigments from absorption spectra, Int. J. Remote Sens., 22(2), 315–338, 2001. 2287

Aiken, J., Fishwick, J. R., Lavender, S. J., Barlow, R., Moore, G., and Sessions, H.: Validation of MERIS reflectance and chlorophyll during the BENCAL cruise October 2002: preliminary validation of new products for phytoplankton functional types and photosynthetic parameters, Int. J. Remote Sens., 28, 497–516, 2007. 2274

Aiken, J., Hardman-Mountford, N. J., Barlow, R., Fishwick, J., Hirata, T., and Smyth, T.: Functional links between bioenergetics and bio-optical traits of phytoplankton taxonomic groups: an overarching hypothesis with applications for ocean colour remote sensing, J. Plankton Res., 30, 165–181, 2008. 2274

Allali, K., Bricaud, A., Babin, M., Morel, A., and Chang, P.: A new method for measuring spectral absorption coefficients of marine particles, Limnol. Oceanogr., 40, 1526–1532, 1995. 2280

Alvain, S., Moulin, C., Dandonneau, Y., and Brèona, F. M.: Remote sensing of phytoplankton groups in case 1 waters from global SeaWiFS imagery, Deep-Sea Res. Pt. I, 52, 1989–2004, 2005. 2274

Alvain, S., Moulin, C., Dandonneau, Y., and Loisel, H.: Seasonal distribution and succession of dominant phytoplankton groups in the global ocean: A satellite view, Global Biogeochemical Cycles, 22, GB3001, ISSN 0886-6236, doi:10.1029/2007GB003154, 2008. 2274

Arrigo, K. R., Robinson, D. H., Worthen, D. L., Schieber, B., and Lizotte M. P.: Bio-optical

properties of the South-Western Ross Sea, J. Geophys. Res., 103, 21683–21695, 1998. 2274

Balch, W. M., Gordon, H. R., Bowler, B. C., Drapeau, D. T., and Booth, E. S.: Calcium carbonate measurements in the surface global ocean based on moderate-resolution imaging spectroradiometer data, J. Geophys. Res., 110, C07001, doi:10.1029/2004JC002560, 2005. 2284, 2290, 2291

Bartlett, J., Voss, K., Sathyendranath, S., and Vodacek, A.: Raman scattering by pure water and seawater, Appl. Opt., 37, 3324–3332, doi:10.1364/AO.37.003324, 1998. 2281

Bovensmann, H., Burrows, J. P., Buchwitz, M., Frerick, J., Nöel, S., Rozanov, V. V., Chance, K. V., and Goede, A. P. H.: SCIAMACHY – mission objectives and measurement modes, J. Atmos. Sci., 56(2), 127–150, 1999. 2283

Bracher, A., Vountas, M., Dinter, T., Burrows, J. P., Röttgers, R., and Peeken, I.: Quantitative observation of cyanobacteria and diatoms from space using PhytoDOAS on SCIAMACHY data, Biogeosciences, 6, 751–764, doi:10.5194/bg-6-751-2009, 2009. 2274, 2279, 2282, 2284, 2285, 2288, 2291, 2292, 2294, 2302

Bricaud, A., Morel, A., and Prieur, L.: Absorption by dissolved organic matter of the sea (yellow substance) in the UV and visible domains, Limnol. Oceanogr., 26, 43–53, 1981. 2280

Bricaud, A., Babin, M., Morel, A., and Claustre, H.: Variability in the chlorophyll-specific absorption coefficients of natural phytoplankton: analysis and parameterization, J. Geophys. Res., 100(13), 321–332, 1995. 2295

Burrows, J. P., Vountas, M., Rozanov, V., Richter, A., Platt U., Haug, H., Marquard, L., and Chance, K.: Study of the Ring effect, Technical Report, ESA Study No. 10996/94/NL/CN, SERCO, 1996. 2279

Bussemer, M.: Der Ring-Effekt: Ursachen und Einfluss auf die spektroskopische Messung stratosphärischer Spurenstoffe, Diploma thesis, Institute of Environmental physics, University of Heidelberg, Germany, 1993. 2279

Carder, K. L., Steward, R. G., Harvey, G. R., and Ortner, P. B.: Marine humic and fulvic acids: their effects on remote sensing of ocean chlorophyll, Limnol. Oceanogr., 34, 68–81, 1989. 2280

Falkowski, P. G., Barber, R. T., and Smetacek, V.: Biogeochemical controls and feedbacks on ocean primary production, Science, 281, 200, 1998. 2273

Gordon, H. R., Brown, O. B., and Jacobs, M. M.: Computed relationships between the inherent and apparent optical properties of a flat homogeneous ocean, Appl. Optics, 14, 417–427,

1975. 2279

Gregg, W. W. and Casey, N. W.: Modeling coccolithophores in the global oceans, Deep Sea Res. Pt. II, 54(5–7), 447–477, 2007. 2286

Gregg, W. W., Ginoux, P., Schopf, P. S., and Casey, N. W.: Phytoplankton and iron: validation of a global three-dimensional ocean biogeochemical model, Deep Sea Res. Pt. II, 50, 3147–3169, 2003. 2286

Hoffmann, L. J., Peeken, I., Lochte, K., Assmy, P., and Veldhuis, M.: Different reactions of southern ocean phytoplankton sizeclasses to iron fertilization, Limnol. Oceanogr., 51(3), 1217–1229, 2006. 2285

Keller, M. D.: Dimethyl sulfide production and marine phytoplankton: the importance of species composition and cell size, Biol. Oceanogr., 6, 375–382, 1989. 2295

Kirk, J. T. O.: Light and Photosynthesis in Aquatic Ecosystems, 2 Edn., Cambridge University Press, ISBN 0 521 45353 4, Cambridge, UK, 1994. 2273, 2279

Longhurst A. R.: Ecological Geography of the Sea, Academic Press, San Diego, CA, 1998. 2295

Mackey, M. D., Mackey, D. J., Higgins, H. W., and Wright, S. W.: CHEMTAX – a program for estimating class abundances from chemical markers: application to HPLC measurements of phytoplankton, Mar. Ecol.-Prog. Ser., 14, 265–283, 1996. 2285

McClain, C. R.: A decade of satellite ocean color observations, Annu. Rev. Marine Sci., 2009.1, 19–42, 2009. 2273

Millie, D. F., Schofield, O. M., Kirkpatrick, G. J., Johnsen, G., Tester, P. A., and Vinyard, B. T.: Detection of harmful algal blooms using photopigments and absorption signatures: a case study of the Florida red tide dinoflagellate, Gymnodinium breve, Limnol. Oceanogr., 42(5, part 2), 1240–1251, 1997. 2274

Mitchell, B. G., Bricaud, A., Carder, K., Cleveland, J., Ferrari, G. M., Gould, R., Kahru, M., Kishino, M., Maske, H., Moisan, T., Moore, L., Nelson, N., Phinney, D., Reynolds, R. A., Sosik, H., Stramski, D., Tassan, S., Trees, C., Weidemann, A., Wieland, J. D., Vodacek, A.: Determination of spectral absorption coefficients of particles, dissolved material and phytoplankton for discrete water samples, edited by: Fargion, G. S., Mueller, J. L., McClain, C. R., Ocean Optics Protocols For Satellite Ocean Color Sensor Validation, Revision 2, NASA Technical Memorandum 2000-209966, Chapter 12, 125–153, 2000. 2280

Morel, A.: Optical modeling of the upper ocean in relation to its biogeneous matter content (case 1 waters), J. Geophys. Res., 93(C9), 10749–10768, 1988. 2282

Morel, A.: Consequences of a Synechococcus bloom upon the optical properties of oceanic case 1 waters, Limnol. Oceanogr., 42, 1746–1754, 1997. 2274

Nair, A., Sathyendranath, S., Platt, T., Morales, J., Stuart, V., Forget, M., Devred, E., and Bouman, H.: Remote sensing of phytoplankton functional types, Remote Sens. Environ., 112, 3366–3375, 2008. 2274

O'Reilly, J. E., Maritorena, S., Mitchell, B. G., Siegel, D. A., Carder, K. L., Garver, S. A., Kahru, M., and McClain, C.: Ocean color chlorophyll algorithms for SeaWiFS, J. Geophys. Res., 103(C11), 24937–24953, 1998. 2273

O'Reilly, J. E., Maritorena, S., Siegel, D. A., O'Brien, M. C., Toole, D., Mitchell, B. G., Kahru, M., Chavez, F. P., Strutton, P., Cota, G. F., Hooker, S. B., McClain, C. R., Carder, K. L., Muller-Karger, F., Harding, L. H., Magnuson, A., Phinncy, D., Moore, G. F., Aiken, J., Arrigo, K. R., Letelier, R., and Culver, M.: Ocean color chlorophyll-a algorithms for SeaWiFS, OC2, and OC4: version 4, in: SeaWiFS Postlaunch Tech. Report Series, edited by: Hooker, S. B. and Firestone, E. R., NASA Technical Memorandum, 2000-206892, Vol. 11, Greenbelt, Maryland: NASA Goddard Space Flight Center (51 pp), 2000. 2274

Perner, D. and Platt, U.: Detection of nitrous acid in the atmosphere by differential optical absorption, Geophys. Res. Lett., 93, 917–920, 1979. 2274, 2275

Platt, T. and Sathyendranath, S.: Oceanic primary production: estimation by remote sensing at local and regional scales, Science, 241, 1613–1620, 1988. 2273

Raven, J. A. and Falkowski, P. G.: Oceanic sinks for atmospheric CO_2, Plant Cell Environ., 22, 741–755, 1999. 2273

Röttgers, R., Haese, C., and Dörffer, R.: Determination of the particulate absorption of microalgae using a point-source integrating-cavity absorption meter: verification with a photometric technique, improvements for pigment bleaching, and correction for chlorophyll fluorescence, Limnol. Oceanogr.-Meth., 5, 1–12, 2007. 2285

Sathyendranath, S. and Platt, T.: Ocean-color model incorporating transspectral processes, Appl. Opt., 37, 2216–2227, doi:10.1364/AO.37.002216, 1998. 2281

Sathyendranath, S., Watts, L., Devred, E., Platt, T., Caverhill, C., and Maass, H.: Discrimination of diatoms from other phytoplankton using ocean-colour data, Mar. Ecol.-Prog. Ser., 272, 59–68, 2004. 2274

Vasilkov, A. P., Joiner, J., Gleason, J., and Bhartia, P.: Ocean Raman scattering in satellite backscatter UV measurements, Geophys. Res. Let., 29, 1837, 4 pp., doi:10.1029/2002GL014955, 2002b. 2279

Vountas, M., Rozanov, V., and Burrows, J. P.: Ring effect: impact of rotational Raman scattering on radiative transfer in earth's atmosphere, J. Quantum Spectrosc. Radiat. Trans., 60, 943–961, 1998. 2279

Vountas, M., Richter, A., Wittrock, F., and Burrows, J. P.: Inelastic scattering in ocean water and its impact on trace gas retrievals from satellite data, Atmos. Chem. Phys., 3, 1365–1375, doi:10.5194/acp-3-1365-2003, 2003. 2279, 2280, 2281, 2282, 2284

Vountas, M., Dinter, T., Bracher, A., Burrows, J. P., and Sierk, B.: Spectral studies of ocean water with space-borne sensor SCIAMACHY using Differential Optical Absorption Spectroscopy (DOAS), Ocean Sci., 3, 429–440, doi:10.5194/os-3-429-2007, 2007. 2279, 2280, 2281, 2282, 2284

Wagner, T., Chance, K., Friess, U., Gil, M., Goutail, F., Hönninger, G., Johnston, P. V., Karlsen-Trnkvist, K., Kostadinov, I., Leser, H., Petritoli, A., Richter, A., Van Roozendael, M., Platt, U.: Correction of the Ring effect and I_0-effect for DOAS observations of scattered sunlight, Proc. of the 1st DOAS Workshop, 13–14 Sep 2001, Heidelberg, Germany, http://joseba.mpch-mainz.mpg.de/pdf_dateien/RING4.pdf, 2001c. 2279

Yassaa, N., Peeken, I., Zöllner, E., Bluhm, K., Arnold, S., Spracklen, D. and Williams, J.: Evidence for marine production of monoterpenes, Environ. Chem., 5, 391–401, doi:10.1071/EN08047, 2008. 2285

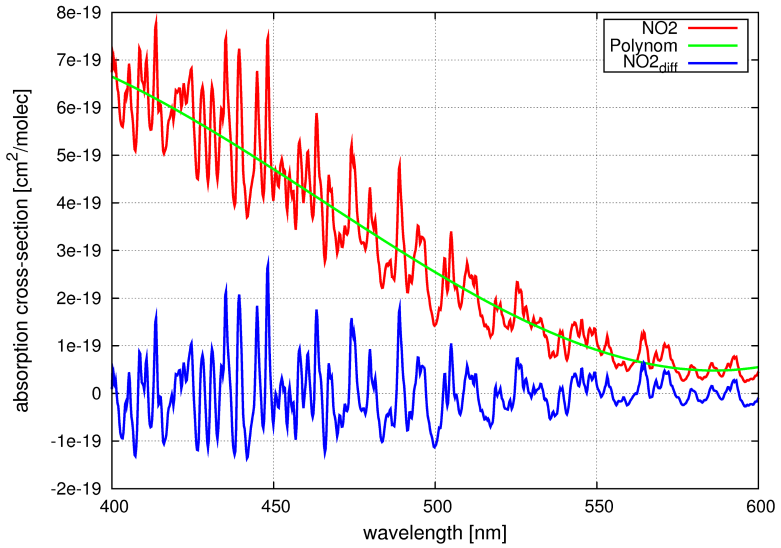

Fig. 1. This figure shows how a given absorption cross-section (here for NO_2) is split into slowly-varying and rapidly-varying (or differential) components. Differential absorption cross-section (blue) of NO_2 has been derived by subtracting a fitted polynomial (green) from the original absorption cross-section (red).

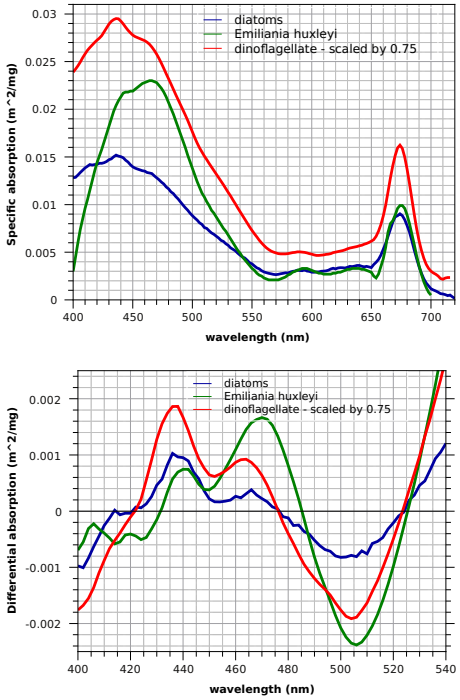

Fig. 2. Upper panel: specific absorption spectra of *E. huxleyi* (green), dinoflagellates (red) and diatoms (blue). The first two spectra were obtained from cultures using a point-source integrating-cavity absorption meter. The latter spectrum was taken from Bracher et al. (2009). Lower panel: differential absorption spectra of three phytoplankton targets. Each of them was derived by subtracting a second order polynomial from the corresponding specific absorption spectrum , which was shown in upper panel.

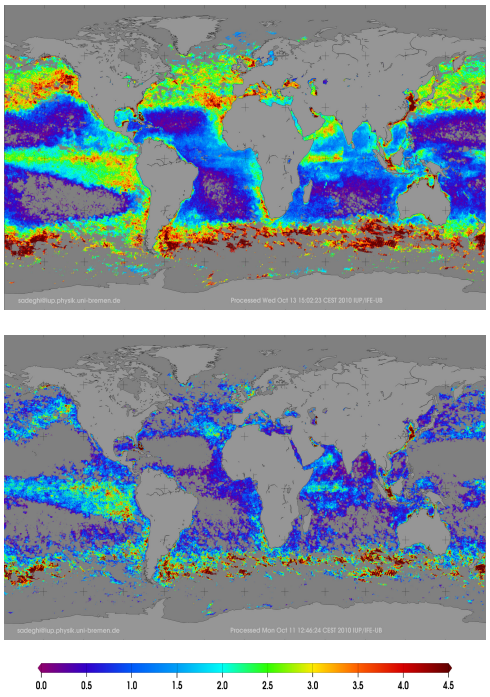

Fig. 3. Global fit-factor maps [mg m^{-2}] for *E. huxleyi* in March 2005, obtained by single-target fit (upper panel) and triple-target fit (lower panel) modes of PhytoDOAS using SCIAMACHY data.

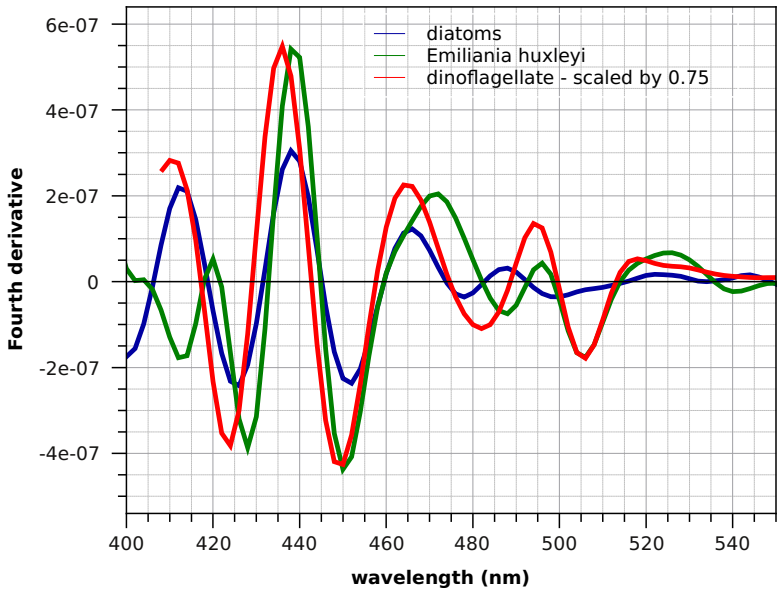

Fig. 4. Fourth derivative curves of the specific absorption spectra of the three PFTs shown in Fig. 2: diatoms (blue), *E. huxleyi* (green) and dinoflagellates (red). The latter curve was scaled to 0.1.

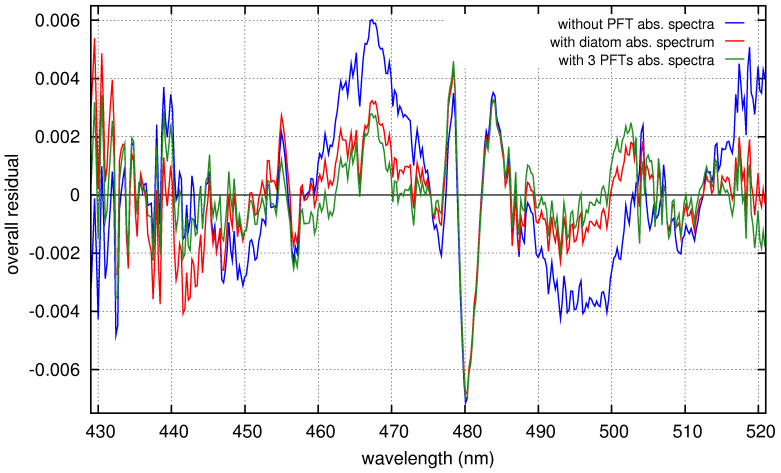

Fig. 5. The improvement to PhytoDOAS was performed by simultaneous fit of the absorption spectra of selected phytoplankton targets in an appropriate wavelength window. This figure compares the overall residuals of the PhytoDOAS retrievals in three different fit-modes: without any PFT target (blue), only with the diatoms abs. spectrum (red) and with the abs. spectra of three selected PFTs (green). All three residual spectra have been obtained via consecutive runs of DOAS for the same SCIAMACHY orbit, passing over North Atlantic (1.07.2005). A sample ground-pixel of this orbit has been taken to plot the residuals, which corresponds to the pixel-center located at 54.51° N and 21.47° W.

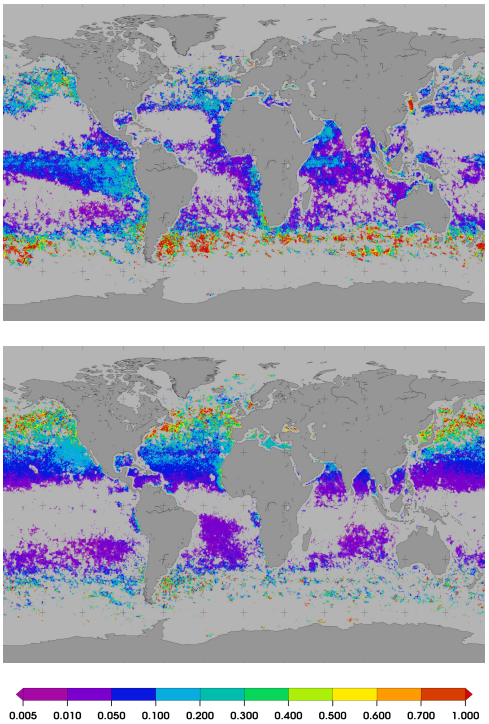

Fig. 6. Global distribution of chl-*a* [mg m^{-3}] for *E. huxleyi* (upper panel) and dinoflagellates (lower panel), retrieved via PhytoDOAS method in the triple-target mode from SCIAMACHY data; monthly averages over *March 2005*.

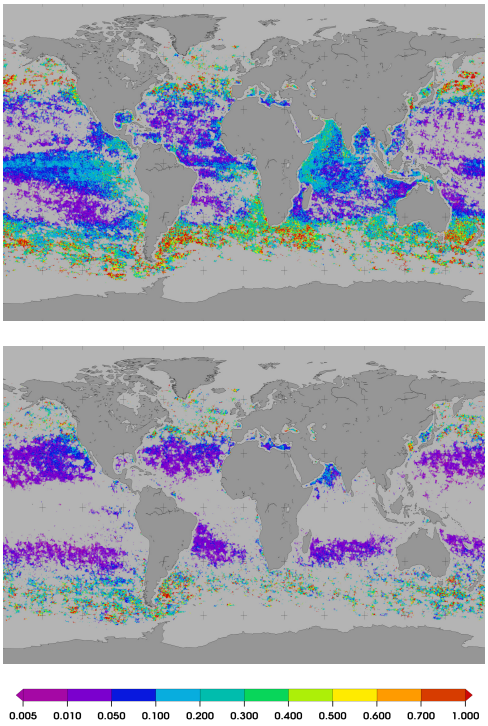

Fig. 7. Global distribution of chl-*a* [mg m^{-3}] for *E. huxleyi* (upper panel) and dinoflagellates (lower panel), retrieved via the PhytoDOAS method in the triple-target mode from SCIAMACHY data; monthly averages over *October 2005*.

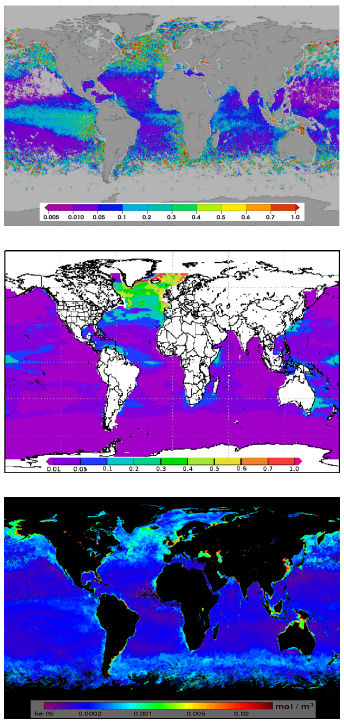

Fig. 8. Comparison of the PhytoDOAS retrieved coccoloithophore chl-*a* [mg m^{-3}] (upper panel) with the NOBM modeled coccolithophore chl-*a* (middle panel), and the global distribution of MODIS-Aqua PIC [mol $CaCO_3$ m^{-3}] (lower panel), all in the northern spring (April/May/June) 2005.

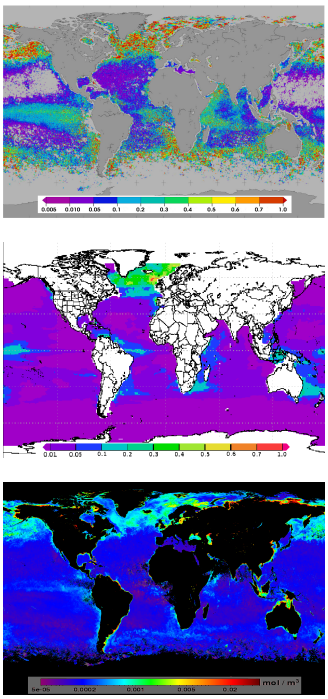

Fig. 9. Comparison of the PhytoDOAS retrieved coccoloithophore chl-*a* [mg m^{-3}] (upper panel) with the NOBM modeled coccolithophore chl-*a* (middle panel), and the global distribution of MODIS-Aqua PIC [mol $CaCO_3$ m^{-3}] (lower panel), all in the northern summer (July/August/September) 2005.

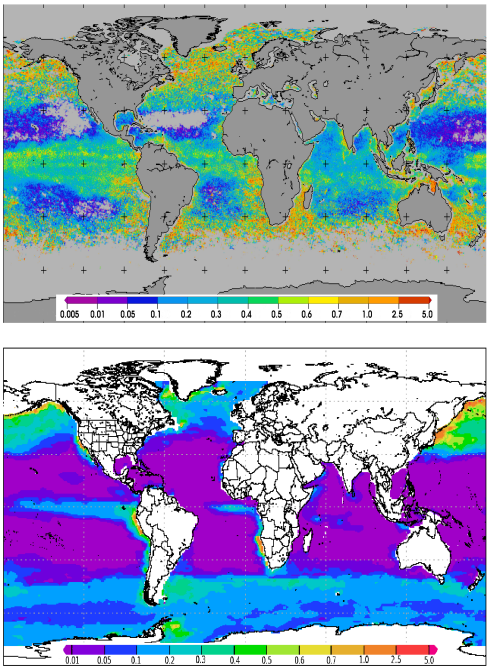

Fig. 10. Comparison of the PhytoDOAS retrieved chl-*a* of diatoms [mg m^{-3}] (upper panel) with the NOBM modeled result of diatom chl-*a* [mg m^{-3}] (lower panel), both in the northern spring (April/May/June) 2005.

Discussion Paper | Discussion Paper | Discussion Paper | Discussion Paper |

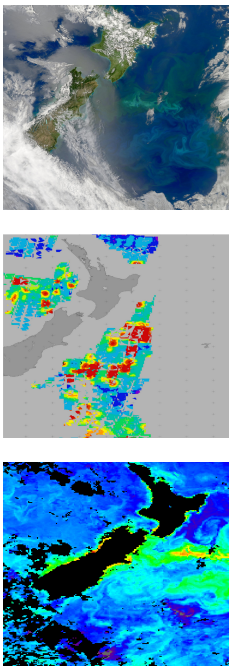

Fig. 11. A case study of phytoplankton bloom detection by PhytoDOAS: the upper panel is a true-color image of MODIS sensor (reported by NASA on 23 December 2009) showing a coccolithophore bloom near Chatham island, on the eastern side of New Zealand. The middle panel depicts the PhytoDOAS retrieval of the coccolithophore chl-*a* for the same region over a period of two weeks (centered at 23 December 2009). The lower panel illustrates the distribution of MODIS-Aqua PIC for the bloom region as a 8-date composite (19 to 26 December 2009).